Referenceless Phase Velocity Mapping Using Balanced SSFP

Jon-Fredrik Nielsen* and Krishna S. Nayak

Phase contrast MRI (PC-MRI) is an established technique for measuring blood flow velocities in vivo. Although spoiled gradient recalled echo (GRE) PC-MRI is the most widely used pulse sequence today, balanced steady state free precession (SSFP) PC-MRI has been shown to produce accurate velocity estimates with superior SNR efficiency. We propose a referenceless approach to flow imaging that exploits the intrinsic refocusing property of balanced SSFP, and achieves up to a 50% reduction in total scan time. With the echo time set to exactly one half of the sequence repetition time (TE = TR/2), we show that non-flow-related image phase tends to vary smoothly across the field-of-view, and can be estimated from static tissue regions to produce a phase reference for nearby voxels containing flowing blood. This approach produces accurate in vivo one-dimensional velocity estimates in half the scan time compared with conventional balanced SSFP phase-contrast methods. We also demonstrate the feasibility of referenceless time-resolved 3D flow imaging (called "7D" flow) in the carotid bifurcation from just three acquisitions. Magn Reson Med 61:1096–1102, 2009.

Key words: MRI velocity mapping; steady state free precession (SSFP); flow quantitation; 7D flow

Phase-contrast (PC) MRI (1–4) is an established technique for measuring blood velocities in vivo and is in wide clinical use. Conventional PC-MRI is based on spoiled gradient recalled echo (GRE) pulse sequences, which provide consistent image quality. Recently, several groups (5–9) have proposed PC techniques based on balanced steady state free precession (SSFP) sequences, which provide accurate velocity measurements with superior SNR efficiency. All of these approaches involve the acquisition of two or more complete datasets, where at least one serves as a phase reference.

In this article, we present a referenceless velocity mapping approach based on balanced SSFP. The method takes advantage of the intrinsic refocusing property of balanced SSFP when the echo time is set to exactly one half of the sequence repetition time (TE = TR/2). Phase-accrual because of resonance offsets is refocused at this point in time (10). The image phase in *static* tissue regions therefore depends only on system-related sources of phase, such as complex receive coil sensitivities, time-delays between gradients and data acquisition, and eddy-current and Maxwell terms. These phase terms vary slowly across the imaging field-of-view (FOV), and can be approximated using a smooth (e.g. low order polynomial) fit in static tissue that is then subtracted from the entire image (11–13). The remaining image phase depends only on local spin velocity and the gradient first moment at the echo. We show that this referenceless approach produces accurate in vivo 1D velocity estimates in half the scan time compared with conventional SSFP phase-contrast methods. We also demonstrate the application of this method to 3D time-resolved flow imaging ("7D" flow) in the carotid bifurcation from only three acquisitions.

METHODS

Pulse Sequences

The proposed technique was applied to both single-slice 1D and volumetric 3D velocity mapping, using balanced SSFP acquisitions with TE = TR/2.

Figure 1 shows the 2DFT acquisition for single-slice 1D velocity mapping along the readout (x) direction. The gradient first moment $m_{1,z}$ in the through-slice (z) direction is nulled at the echo. The shaded region indicates the gradient area responsible for flow encoding; note that it is the readout gradient itself that encodes velocity, and *not* an additional bipolar pulse (7).

Figure 2 shows the three 3DFT acquisitions used for volumetric mapping of full velocity vectors. Each acquisition has a different gradient first moment at the echo: Acquisition A has non-zero $m_{1,x}^{\mathrm{A}}$ and $m_{1,z}^{\mathrm{A}}$; acquisition B has non-zero $m_{1,x}^{\mathrm{B}}$ and $m_{1,z}^{\mathrm{B}}$; and acquisition C has non-zero $m_{1,y}^{\mathrm{C}}$ and $m_{1,z}^{\mathrm{C}}$.

Background Phase Subtraction

In each 2DFT/3DFT dataset, 2D/3D regions-of-interest (ROIs) were defined manually inside static tissue and in close proximity to the vessel of interest. Care was taken to exclude fat from these ROIs, because fat may be in an SSFP band where the phase is refocused to π rather than 0, due to the fat/water chemical shift (−440 Hz at 3T). The image phase $\Theta(\mathbf{r})$ inside the ROIs was fitted to a low-order 2D/3D polynomial, using the mean-squared error as a goodness-of-fit criterion. A low-order polynomial was chosen because it has been shown to provide a good local fit to the smoothly varying background phase in MRI images (11,12). Finally, the polynomial phase fit was subtracted from the image phase, resulting in a phase image that depends only on

Magnetic Resonance Engineering Laboratory, Ming Hsieh Department of Electrical Engineering, University of Southern California, Los Angeles, California

Grant sponsor: American Heart Association; Grant number: POST-0625253Y; Grant sponsor: National Institutes of Health; Grant numbers: R01-HL074332, R21-HL079987

*Correspondence to: Jon-Fredrik Nielsen, PhD, Biomedical Engineering, University of Michigan, 2360 Bonisteel Ave, Ann Arbor, MI 48109 - 2108. E-mail: jfnielse@umich.edu

Received 22 February 2008; revised 26 August 2008; accepted 19 October 2008.

DOI 10.1002/mrm.21884

Published online 19 February 2009 in Wiley InterScience (www.interscience.wiley.com).

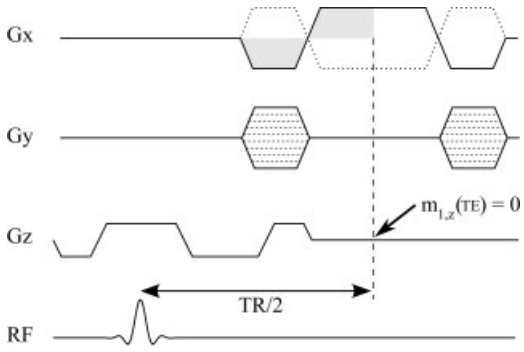

FIG. 1. SSFP pulse sequence for single-slice (2DFT) referenceless 1D velocity mapping along the readout (x) direction. The through-plane gradient first moment $m_{1,z}$(TE) is nulled at TE = TR/2. Gradient amplitudes are not drawn to scale.

the gradient first moment at the echo and the local spin velocity.

Experimental Methods

All experiments were performed in healthy volunteers on a commercial 3T scanner (Signa Excite HD, GE Healthcare, Waukesha, WI) with maximum gradient amplitude and slew rate of 40 mT/m and 150 T/m/s, respectively, and with 250 kHz receiver bandwidth. All subjects provided informed consent, and were scanned using a protocol approved by our Institutional Review Board. Table 1 summarizes the scan parameters used in the three experiments described below.

In the 2DFT imaging experiments, the RF and imaging gradients were applied continuously, such that a steady-state was reached for static spins. To mitigate RF heating in the 7D flow experiment, acquisition was triggered by each ECG R-wave, and occurred for only the first half of each cardiac cycle. An 8-TR Kaiser-ramp preparation was used to minimize transient signal oscillations (14).

Experiment 1: Smoothness of Background Phase

To assess the nature of background phase patterns in clinical MRI velocity mapping applications, balanced 2DFT SSFP images were obtained in the femoral bifurcation using a single-channel birdcage quadrature knee coil; in the carotid bifurcation using a 4-channel carotid surface coil array; and in the abdominal aorta using an 8-channel cardiac surface coil array. The phase in single-coil images from each of these acquisitions was fitted to polynomials of order 1 through 4, and the goodness-of-fit was evaluated.

Experiment 2: Accuracy of Velocity Measurements

To assess the performance of the proposed approach compared to conventional SSFP PC-MRI, single-slice 1D velocity mapping of the common carotid artery was performed in one healthy volunteer using the sequence in Fig. 1. The common carotid artery was oriented in-plane, with the readout (x) oriented along the S/I direction. A total of 20 images were acquired: 10 images were acquired with a positive readout gradient during data acquisition (solid "Gx" line in Fig. 1), and 10 images were acquired with the readout gradient inverted (dotted "Gx" line in Fig. 1). This data was then reconstructed in two ways: First, 10 PC maps were generated by performing conventional PC processing, i.e., by calculating the phase-difference between two images acquired with opposite sign of the readout gradient. This corresponds to the gradient inversion method proposed by Markl et al. (6), applied to velocity encoding along the readout direction, as implemented by Grinstead and Sinha (7). Constant and linear background offsets were removed from each of the 10 PC images, by performing a linear plane fit to the same static ROI that was used for referenceless velocity mapping. Second, 20 velocity maps were calculated using the proposed referenceless processing, by calculating the velocity directly from the residual image phase

$$\Theta(\mathbf{r}) = \gamma v_x(\mathbf{r}) m_{1,x}(TE) \qquad [1]$$

Note that flow along the phase-encode (y) direction does not affect the image phase, but rather manifests as a spatial shift along y. For example, for a square phase-encode gradient pulse of amplitude 2 G/cm and a spatial resolution of 1 mm, a velocity of 100 cm/s along the phase-encode direction will result in a shift of 0.29 pixels.

Velocity estimates from the two methods were compared in terms of accuracy and velocity SNR. The noise σ_v in the

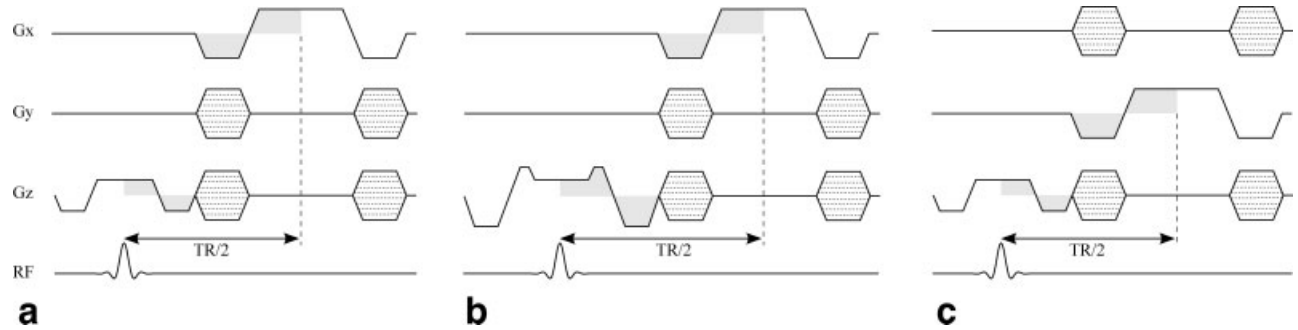

FIG. 2. SSFP pulse sequence for volumetric (3DFT) referenceless 3D velocity mapping ("7D" flow mapping). Acquisition A is a conventional 3DFT SSFP sequence with TE = TR/2. Acquisition B is similar to A, but has a different first moment $m_{1,z}$ along z. Acquisition C is identical to A, except that the readout and phase-encode directions are swapped. The shaded areas indicate the gradient segments responsible for flow-encoding.

Table 1
Scan Parameters for the Three Experiments Performed in This Study

	Experiment 1 Background Phase	Experiment 2 Accuracy	Experiment 3 7D flow
Pulse sequence	2DFT SSFP (FIESTA)	Fig. 1	Fig. 2
Receive coil	Knee; carotid; cardiac	Carotid	Carotid
TE/TR	2.506/5.012 ms	2.978/5.956 ms	3.322/6.644 ms
Matrix size	160×160	160×160	$160 \times 120 \times 30$
FOV	16×16 cm^2	16×16^a cm^2	$16 \times 12 \times 6$ cm^3
Slice/slab thickness	7 mm	7 mm	60 mm
Voxel size	$1 \times 1 \times 7$ mm^3	$1 \times 1 \times 7$ mm^3	$1 \times 1 \times 2$ mm^3
Readout direction	S/I	S/I	R/L and A/P
Flip angle	50°	40°	50°
RF phase cycling	(0°, 180°)	(0°, 180°)	(0°, 180°)
Views per cardiac phase	8	8	8
Total scan duration	20 sec	20 sec per repetition	22 mins
Transient catalyzation	none (continuous)	none (continuous)	8-tip Kaiser ramp
Results	Fig. 3 and Table 2	Fig. 4 and Table 3	Figs. 5 and 6

[a]When imaging the abdominal aorta, an FOV of 16×35 cm^2 was used.

1D velocity maps obtained with the proposed method is determined by the phase noise σ_Θ in the SSFP image, and by the gradient first moment at the echo:

$$\mathrm{SNR}_v = \frac{v}{\sigma_v} = \frac{\Theta}{\sigma_\Theta} \quad [2]$$

In this experiment, the maximum encoded velocity (VENC) for PC reconstruction is half of that of the referenceless reconstruction, which results in twice the velocity signal. Subtracting two phase images with uncorrelated phase noise σ_Θ results in a $\sqrt{2}$ increase in the phase noise $\sqrt{\sigma_\Theta^2 + \sigma_\Theta^2} = \sqrt{2}\sigma_\Theta$ for PC reconstruction. The velocity SNR for PC and referenceless velocity mapping is therefore expected to follow:

$$\mathrm{SNR}_v^{\mathrm{PC}} = \frac{v^{\mathrm{PC}}}{\sigma_v^{\mathrm{PC}}} = \frac{2\Theta}{\sqrt{2}\sigma_\Theta} = \sqrt{2}\mathrm{SNR}_v \quad [3]$$

where SNR_v and SNR_v^{PC} represent the velocity SNR for the proposed method and PC, respectively. Velocity noise was calculated for each pixel within the static ROI by calculating the standard deviation of all 10 (PC) or 20 (referenceless) measurements. The final noise estimate was obtained by calculating the mean noise and standard error of the mean noise from all pixels within the ROI.

Experiment 3: Feasibility of Referenceless 7D Velocity Mapping

To determine whether referenceless SSFP velocity imaging could be applied to flow field measurements, time-resolved 3D velocity mapping was performed in the carotid bifurcation of a healthy volunteer, using the sequences in Fig. 2. The imaging slab was oriented axially, with partition-encoding (z) oriented along the S/I direction.

The velocity was calculated from the image phase in each of the three acquisitions,

$$\Theta^{\mathrm{A}} = \gamma v_x m_{1,x}^{\mathrm{A}} + \gamma v_z m_{1,z}^{\mathrm{A}} \quad [4]$$

$$\Theta^{\mathrm{B}} = \gamma v_x m_{1,x}^{\mathrm{B}} + \gamma v_z m_{1,z}^{\mathrm{B}} \quad [5]$$

$$\Theta^{\mathrm{C}} = \gamma v_y m_{1,y}^{\mathrm{C}} + \gamma v_z m_{1,z}^{\mathrm{C}} \quad [6]$$

These equations were solved for the velocity vector components v_x, v_y, and v_z, resulting in a volumetric data set with a 3D velocity vector for each voxel at each time step. This data set was visualized in two ways: (1) By producing 3D flow streamlines at the time of peak flow and (2) by generating time-resolved particle traces ("pathlines"). Streamlines were generated by selecting a set of seed points, and drawing line segments of length 0.2 pixels successively along the direction of the local velocity vector. To facilitate these calculations, a continuous velocity vector field was generated from the discrete $160 \times 120 \times 30$ velocity grid by trilinear interpolation between the nearest grid points. Each streamline was terminated if the local streamline angle exceeded 30°. Pathlines were calculated in a similar manner, except that the step size reflected the physical distance traveled by a massless particle moving with the fluid. By interrupting the pathlines at different points in time, we generated a movie depicting the physical fluid flow. Streamline and pathline results were visualized using a graphical software tool built in-house using Java (Sun Microsystems, Santa Clara, CA).

RESULTS

Smoothness of Background Phase

Figure 3 shows the image phase for three different vascular regions at the time of peak flow. Before background phase subtraction, the phase in static tissue is substantial. After fitting a smooth function to phase within the marked ROIs and subtracting this fit from the entire image, the residual phase in static tissue is close to zero. Table 2 lists

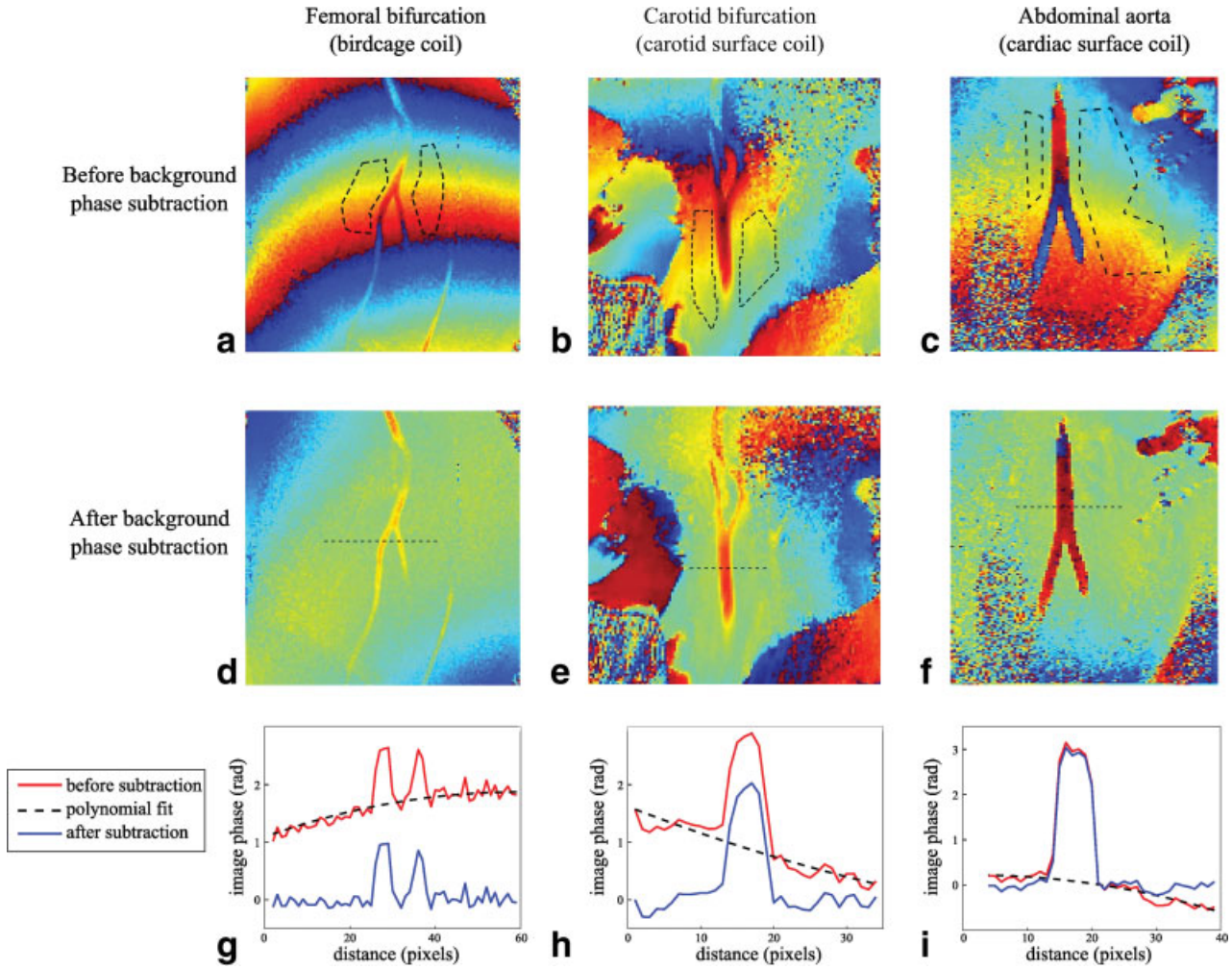

FIG. 3. Smoothness of background phase in balanced SSFP imaging with TE = TR/2. Image phase before (top row) and after (middle row) background phase subtraction using a 2nd order polynomial fit. Bottom row: phase along the dashed horizontal line indicated in (**d–f**), both before (red) and after (blue) background phase subtraction. The 2nd order polynomial fit is indicated by the dashed line in each plot. Nonzero image phase observed inside the arteries arises in (d–f) from the intrinsic flow-encoding caused by the readout gradient, and provides a direct measure of blood flow velocity. The readout direction is vertical in all images.

the phase standard deviation inside static ROIs after polynomial fitting of order 1, 2, 3, and 4, for three different anatomical regions, and for two different subjects for each anatomical region. The least-squares fitting routine used in our work results in mean errors over the background ROI that are close to zero regardless of polynomial order, and we therefore chose the phase RMS value as a measure of goodness-of-fit. Generally, the goodness-of-fit increases with higher order fitting. However, 4th order fitting produces only marginal improvements over 3rd order fitting. Furthermore, in each case the phase standard deviation for 2nd order fitting was within 11% of the value obtained with

Table 2
Phase Standard Deviation (Radians) in Static Tissue ROIs Following Polynomial Fitting (Experiment 1)

	1st Order	2nd Order	3rd Order	4th Order
Femoral artery, subject 1	0.154	0.116	0.111	0.110
Femoral artery, subject 2	0.130	0.111	0.110	0.110
Carotid artery, subject 1	0.123	0.112	0.101	0.095
Carotid artery, subject 2	0.162	0.148	0.141	0.133
Abdominal aorta, subject 1	0.206	0.161	0.147	0.147
Abdominal aorta, subject 2	0.217	0.211	0.203	0.198

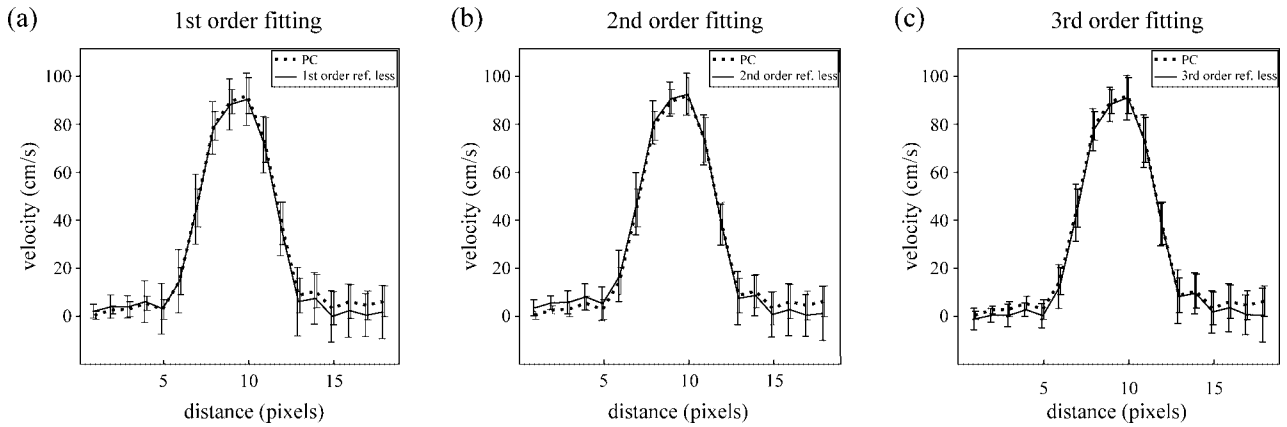

FIG. 4. Accuracy of referenceless velocity measurements. (**a**–**c**) Spatial velocity profiles across the common carotid artery in mid-systole, obtained using conventional balanced SSFP phase-contrast processing (dotted curve), and the proposed referenceless method (solid curve) using (a) 1st, (b) 2nd, and (c) 3rd order polynomial fitting. In each case, the dotted and solid curves are in excellent agreement.

3rd order fitting. These results indicate that local background phase can typically be adequately approximated by a 3rd or lower order polynomial for the carotid and femoral bifurcations and the abdominal aorta; it is our expectation that most other locations will provide similar results.

Accuracy of Velocity Measurements

Figure 4 summarizes the results of performing 1D velocity mapping in the common carotid artery of a healthy volunteer, using PC processing and the proposed method with either 1st, 2nd, or 3rd order polynomial fitting. The error bars indicate the standard deviation over all 10 measurements (for PC) or 20 measurements (for the proposed method). In all cases, referenceless velocity estimates inside the vessel lumen are in good agreement with the PC values.

Table 3 lists the measured velocity noise for referenceless and PC imaging. The noise increase due to referenceless processing is close to the theoretically expected value of $\sqrt{2}$.

Feasibility of Referenceless 7D Velocity Mapping

Figure 5 shows velocity streamlines calculated from 7D flow measurements in the carotid bifurcation of a healthy volunteer, using data from one receive channel. The streamlines are color-coded such that the red, green, and blue components equal $v_x/|v|$, $v_y/|v|$, and $v_z/|v|$, respectively, where $|v| = \sqrt{v_x^2 + v_y^2 + v_z^2}$. Blood flow is clearly observed through the common carotid artery (CCA), and subsequently through the internal and external carotid arteries. Figure 5c nicely shows rotational flow originating in the carotid bifurcation, which is a normally occurring flow pattern in healthy individuals.

Table 3
Velocity Noise for PC and Referenceless Measurements (Experiment 2)

	PC	1st order	2nd order	3rd order
σ_v (cm/s)	6.87 ± 0.89	11.26 ± 0.92	10.13 ± 0.80	9.83 ± 0.80
σ_v/σ_v^{PC}	1	1.64 ± 0.25	1.47 ± 0.23	1.43 ± 0.22

The theoretically expected noise increase due to referenceless processing is $\sqrt{2} = 1.414$ (see Eq. [3]).

Figure 6 shows pathlines generated from the 7D flow dataset, during a 95 ms systolic time-period. Flow in the ECA is mostly vertical (blue) and unidirectional (100+25 ms, arrow). Flow in the ICA is more complex, and appears to consist of two separate paths: (1) Rotational flow (100+35 ms, curved arrow), and (2) simpler, mostly upward flow in the lumen interior (100+35 ms, straight arrow). At 100+45 ms, the curved pathlines switch direction rapidly upwards (100+45 ms, curved arrow).

DISCUSSION

We have demonstrated that SSFP image phase in static regions is often spatially smooth, and that subtraction of the background phase estimated from static regions in close proximity to vessels of interest can enable accurate blood flow velocity measurements without a phase reference. The proposed method relies on the intrinsic spin-echo-like refocusing property of balanced SSFP (10), and on background phase removal using a low-order polynomial fit (11,12).

Accurate background phase estimation may be difficult to achieve in imaging applications that contain little or no static tissue near the vessel. One important example is cardiac flow imaging, where the heart chambers are surrounded by myocardium that is in constant motion. It may be possible to estimate background phase from the anterior and posterior chest walls, but the accuracy of background phase estimates inside the heart (far from the chest walls) would need to be checked carefully. Alternatively, one could derive background phase estimates from myocardial tissue in a relatively stable cardiac phase (e.g., mid-diastole or end-systole).

Markl et al. (15) and Markl and Pelc (16) showed that in 2DFT balanced SSFP imaging, off-resonant spins moving through-plane can undergo significant transient oscillations, resulting in image artifacts. These oscillations show a complicated dependence on flow rate, flip angle, slice

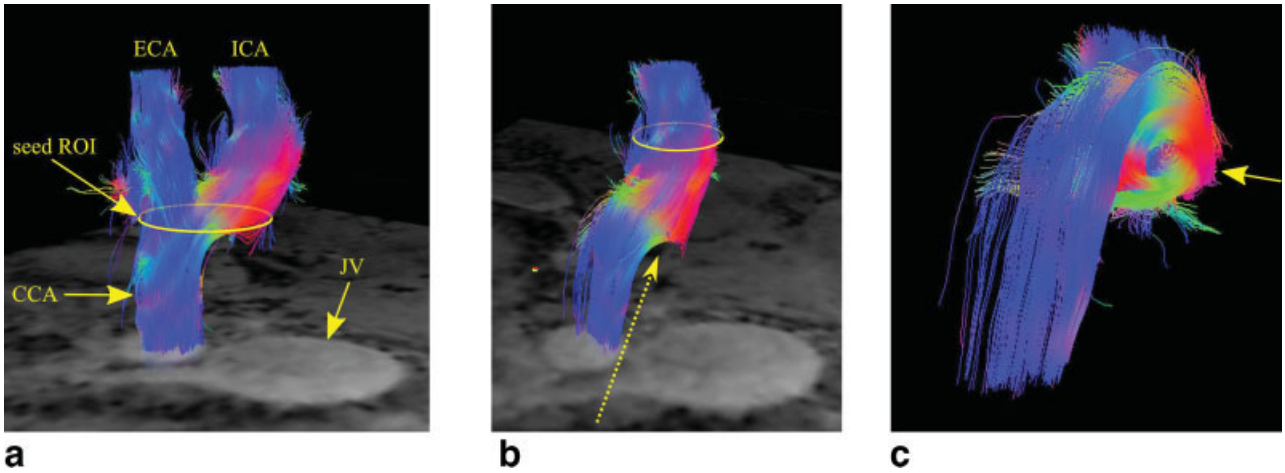

FIG. 5. Feasibility of referenceless 7D flow mapping in the carotid bifurcation. (**a**) 3D streamlines at mid-systole emanating from points within the 2D cross-sectional "seed" ROI (yellow oval). A gray-scale 2D axial magnitude image is shown for reference. (**b**) Streamlines emanating from a seed ROI in the ICA. (**c**) The same streamlines shown in (b), viewed along the direction indicated by the arrow in (b).

thickness and profile, and degree of off-resonance. SSFP PC imaging may be relatively immune to these oscillations, as long as the same transient behavior is reproduced every R-R interval. The method proposed here relies on the absolute spin phase, and transient phase oscillations may therefore cause errors in the measured velocities for off-resonance spins. Transient oscillations are unlikely to have had a significant role in the experiments performed in this study. A good shim was obtained in all cases, and the most rapid flow occurred either in-plane or through a 6-cm 3DFT slab.

The sequence repetition time is an important consideration in balanced SSFP imaging, and should generally be kept as short as possible to maximize the separation between signal nulls in the SSFP spectral profile. The TR of the 1D velocity mapping sequence in Fig. 1 is slightly longer than a conventional SSFP imaging sequence with the same sequence parameters, due to the additional gradients required to null the first moment $m_{1,z}$ at the echo, and the requirement that TE = TR/2. This is a drawback of the proposed method. The TR of acquisition B in the 7D flow sequence shown in Fig. 2 is also longer than that of

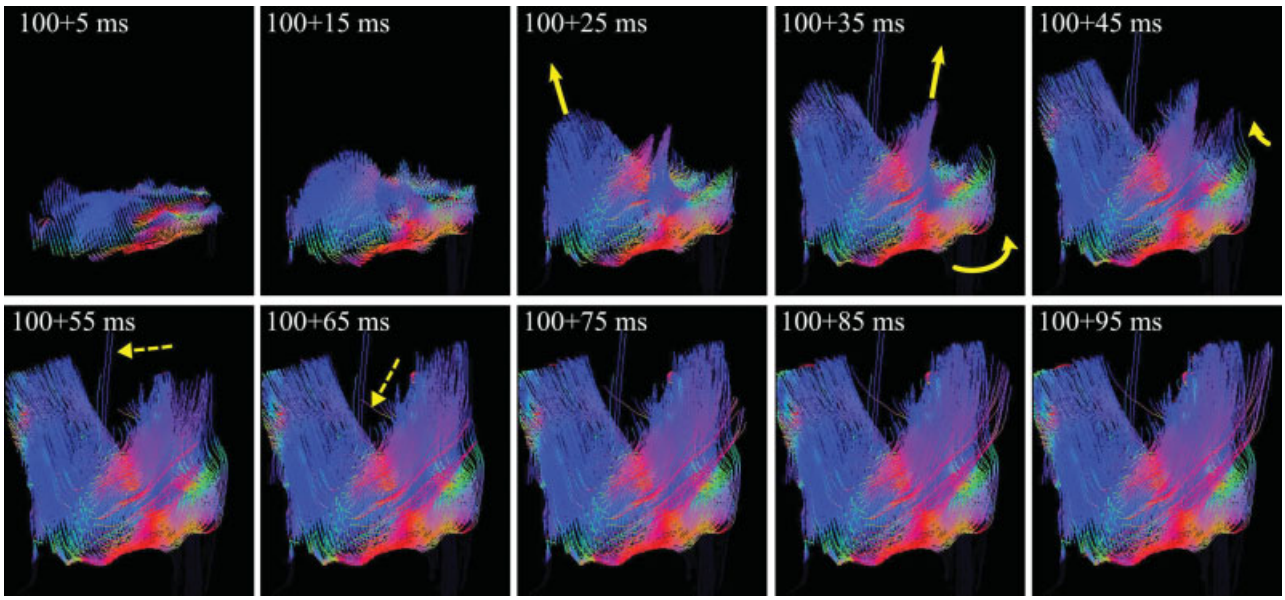

FIG. 6. Pathline visualization of the 7D carotid flow dataset. Pathlines originate from an axial plane at the height of the carotid bifurcation (see seed ROI in Fig. 5a), and were initiated 100 ms after the cardiac ECG trigger. The view angle is approximately the same as in Fig. 5a. The images show particle traces over the course of the subsequent 95 ms. The time indicated in each frame is the total time elapsed since the ECG trigger. Solid arrows indicate the local flow direction at a few select locations and time-points (see main text). Dashed arrows point to pathlines that erroneously leave the vessel lumen.

an equivalent conventional SSFP-PC acquisition, but may be reduced by applying the principle of gradient inversion along the slice-select direction (6).

In 2DFT and 3DFT imaging, local resonance offsets cause spatial shifts along the readout (frequency-encoding) direction. In the velocity mapping sequence shown in Fig. 2, acquisition C produces a spatial shift along the physical y-direction, whereas acquisitions A and B produce a shift along x. These shifts can be minimized with improved shimming over the ROI, and by using the maximum available gradient amplitude during the readout.

The method introduced here is related to the nonsubtractive spiral GRE velocity mapping technique proposed by Man et al. (12). Their method relies on the assumption that flow-related phase is confined to structures containing high spatial-frequency components, and that image phase due to all other sources (including resonance offsets) is smoothly varying. By using spiral readouts with a short TE (3–4 ms) and a combination of low-order polynomial fitting and low-pass filtering of the image, Man et al. demonstrated nonsubtractive 1D velocity mapping with good accuracy. When compared with the method of Man et al. the method proposed here uses SNR-efficient balanced SSFP 2DFT/3DFT acquisitions that avoid the resonance-offset-induced blurring associated with spiral acquisitions, and ensure that the background phase is independent of local resonance offset.

CONCLUSIONS

The proposed method exploits the intrinsic "spin-echo like" refocusing property of balanced SSFP (10) to achieve velocity-mapping in shorter scan times compared with conventional SSFP phase-contrast methods. In vivo 1D velocity mapping measurements obtained with the proposed technique are in excellent agreement with those obtained using SSFP PC-MRI, and are acquired in half the time. "7D" velocity mapping using three 3DFT image acquisitions has also been demonstrated as feasible.

ACKNOWLEDGMENTS

The authors thank Hsu-Lei Lee for help implementing sequences for initial preparation of the steady state, and Tzung Hsiai for interpretation of the 7D carotid flow results.

REFERENCES

1. Hahn EL. Detection of sea-water motion by nuclear precession. J Geophys Res 1960;65:776–777.
2. Moran PR. A flow velocity zeugmatographic interface for NMR imaging in humans. Magn Reson Imaging 1982;1:197–203.
3. Pelc NJ, Herfkens RJ, Shimakawa A, Enzmann DR. Phase-contrast cine magnetic resonance imaging. Magn Reson Q 1991;7:229–254.
4. Pelc NJ, Sommer FG, Li KC, Brosnan TJ, Herfkens RJ, Enzmann DR. Quantitative magnetic resonance flow imaging. Magn Reson Q 1994;10:125–147.
5. Overall WR, Nishimura DG, Hu BS. Fast phase-contrast velocity measurements in the steady state. Magn Reson Med 2002;48:890–898.
6. Markl M, Alley MT, Pelc NJ. Balanced phase-contrast steady-state free precession (PC-SSFP): A novel technique for velocity encoding by gradient inversion. Magn Reson Med 2003;49:945–952.
7. Grinstead J, Sinha S. In-plane velocity encoding with coherent steady-state imaging. Magn Reson Med 2005;54:138–145.
8. Pai VM. Phase contrast using multiecho steady-state free precession. Magn Reson Med 2007;58:419–424.
9. Nielsen JF, Nayak KS. SSFP and GRE phase contrast imaging using a three-echo readout. Magn Reson Med 2007;58:1288–93.
10. Scheffler K, Hennig J. Is trueFISP a gradient-echo or a spin-echo sequence? Magn Reson Med 2003;49:395–397.
11. Bernstein MA, Perman WH. Least-squares algorithm for phasing MR images. In Proceedings of SMRM, 6th Annual Meeting, New York, 1987, 801.
12. Man LC, Pauly JM, Nishimura DG, Macovski A. Nonsubtractive spiral phase contrast velocity imaging. Magn Reson Med 1999;42:704–713.
13. Rieke V, Vigen KK, Sommer G, Daniel BL, Pauly JM, Butts K. Referenceless PRF shift thermometry. Magn Reson Med 2004;51:1223–1231.
14. Le Roux P. Simplified model and stabilization of SSFP sequences. J Magn Reson 2003;163:23–37.
15. Markl M, Alley MT, Elkins CJ, Pelc NJ. Flow effects in balanced steady state free precession imaging. Magn Reson Med 2003;50:892–903.
16. Markl M, Pelc NJ. On flow effects in balanced steady-state free precession imaging: Pictorial description, parameter dependence, and clinical implications. J Magn Reson Imaging 2004;20:697–705.